Dalton Transactions

Accepted Manuscript

ROYAL SOCIETY OF CHEMISTRY

www.rsc.org/dalton

Enhanced visible light photocatalytic activity of $ZnIn_2S_4$ modified by semiconductors

Sai Yang[a] Li Li[b] Wenhui Yuan[a*] Zilong Xia[a]

To improve the visible light photocatalytic activity of $ZnIn_2S_4$ sample, we synthesized two kinds of coupled-photocatalysts: TiO_2@$ZnIn_2S_4$ core-shell type heterostructure composites by a simple and flexible hydrothermal route using TiO_2 as precursors and CuO/$ZnIn_2S_4$ contact type heterostructure composites incorporated with different amounts of CuO by the impregnation-calcination method. These as-prepared samples were characterized by X-ray diffraction (XRD), scanning electron microscopy (SEM), transmission electron microscopy (TEM), UV-Visible absorption spectra (UV-Vis) and nitrogen adsorption measurements. The enhancement of photocatalytic activity was observed after the addition of TiO_2 and CuO. It was found that the as-synthesized TiO_2@$ZnIn_2S_4$ photocatalyst was more efficient than TiO_2 and $ZnIn_2S_4$ in the photocatalytic degradation of methylene blue (MB). TEM images confirmed the TiO_2@$ZnIn_2S_4$ nanoparticles possessed well-proportioned core-shell morphology. On the other hand, the effects of CuO loading amount on the crystal structure, and photocatalytic property of CuO/$ZnIn_2S_4$ samples for MB degradation under visible light irradiation were investigated, suggesting the introduction of CuO could influence the morphology, BET specific surface area of $ZnIn_2S_4$ sample and enhanced visible light absorption of photocatalysts. The photocatalytic degradation performance of MB was remarkably improved in the presence of CuO/$ZnIn_2S_4$ compared to pure $ZnIn_2S_4$ and 10 mol% CuO/$ZnIn_2S_4$ was found to possess the optimal photocatalytic

*Corresponding author. Tel: +86 20 8711 1887; fax: +86 20 8711 1887. E-mail address: cewhyuan@scut.edu.cn
Present Address: School of Chemistry and Chemical Engineering, South China University of Technology, Wushan, Tianhe, Guangzhou 510640, P. R. China.

performance. Moreover, mechanisms for the enhanced photocatalytic activity over the TiO_2@$ZnIn_2S_4$ and CuO/$ZnIn_2S_4$ composites were proposed.

Keywords: TiO_2@$ZnIn_2S_4$; CuO/$ZnIn_2S_4$; Heterostructures; Characterization; Mechanism

Introduction

With the development of modern industry, synthetic dyes are being extensively used in various branches related to leather, plastic, textile, and other industry [1]. Colorful dyes have enriched our lives but also have negatively affected the environment such as a serious pollution concern because many of them are carcinogenic, mutagenic, and even toxic to human beings and other species. For the treatment of wastewater, the degradation of organic dyes by a photocatalytic approach is found to be applicable [2]. Nowadays, photocatalysis is widely used as a "green" technology in the field of environmental remediation and energy conversion [3-5], which provides a promising approach for the decomposition of synthetic dyes owing to its high efficiency, low-cost, and long-term stability against chemical and/or photocorrosion [6]. The photocatalytic organic pollutants degradation over semiconductor photocatalysts has attracted increasing attention with environmental remediation and renewable energy production [7-9]. The great present interest is to use solar light which is free and inexhaustible. Therefore, a technology utilizing renewable energy such as solar energy is one of the best and most sustainable options.

$ZnIn_2S_4$ has recently attracted considerable attention for its strong photocatalytic activity for water splitting and the oxidative decomposition of organic contaminants under visible light. Numerous methods have been used to synthesize $ZnIn_2S_4$ materials with various morphologies (i.e. nanotubes, nanoribbons, nanowires, and

flower-like microspheres) and improve the performance of $ZnIn_2S_4$ materials for photocatalytic water reduction. Single $ZnIn_2S_4$ or Zn-In-S composites were synthesized by a NaCl-assisted method [10-11] and homogeneous $ZnIn_2S_4$ nano/micropeony spheres have been prepared through a solvothermal method and exhibited good performance for efficient photodegradation of methylene blue under visible-light irradiation [12]. Moreover, the effects of adding surfactants (i.e. CTAB) [13] on photocatalytic performance of $ZnIn_2S_4$ materials were also investigated in details. However, the photocatalytic activity of pure $ZnIn_2S_4$ is low because of its poor visible light adsorption and difficult electron-hole pair separation. Many attempts have been made to improve the photocatalytic activity of $ZnIn_2S_4$. To solve this problem, on the one hand, some doped $ZnIn_2S_4$ photocatalysts (i.e. Cu, Co metals-doped) were developed in order to enhance the H_2 evolution activity [14-15]. On the other hand, $ZnIn_2S_4$-based composite photocatalysts have also been investigated, such as MWCNTs/$ZnIn_2S_4$ [16], CdS/$ZnIn_2S_4$ [17], $CuInS_2$/$ZnIn_2S_4$ [18], In_2S_3/$ZnIn_2S_4$ [19], RGO/$ZnIn_2S_4$ [20]. However, the photocatalytic properties of $ZnIn_2S_4$-based composite photocatalysts coupled with other semiconductors have not been investigated extensively.

As we all know, microstructure of catalysts can strongly influence catalytic performance, so controlling the morphological properties of catalyst materials during synthesis process is of great importance. It was reported that constructing heterostructures was a quite effective method to improve the photocatalytic activity, and heterostructures were proved to have great effect on electron transfer [21-22]. By coupling or capping a semiconductor with another semiconductor, which two semiconductor particles have different energy levels, it is possible to design semiconductor heterostructures. Photoinduced charge transfer processes in two-

component semiconductor particulate systems can improve the efficiency of charge separation. Considerable interest has been focused on studying semiconductor heterostructure systems, and a variety of capped and coupled semiconductor systems have been reported. Coupled semiconductor systems include CuO/WO_3 [23], CuO-$BiVO_4$ [24] and capped semiconductor systems such as well-defined core-shell $Au@TiO_2$ hollow spheres [25], and $ZnO/CuInS_2$ core-shell composites [26] have been synthesized. Such capped and coupled semiconductor systems not only extended the photoresponse but also rectified the flow of photogenerated charge carriers and enhanced the photocatalytic efficiency of these photocatalysts [27]. $ZnIn_2S_4$ was modified by other semiconductors with suitable band edges to form a heterojunction photocatalyst which results in enhancing the photocatalytic activity of $ZnIn_2S_4$ through a synergistic effect.

The objective of this work is to couple two semiconductors ($ZnIn_2S_4$ and another suitable semiconductor) with higher and lower CB and VB energy values to allow for more efficient charge carrier separation, resulting in induced charge separation in $ZnIn_2S_4$. So we synthesized two different composite materials: $TiO_2@ZnIn_2S_4$ capped semiconductor system through the one-step hydrothermal method; $CuO/ZnIn_2S_4$ coupled semiconductor system by the impregnation-calcination method, by which the photocatalyst may minimize the recombination of photoexcited electron-hole pairs during photocatalysis, thereby increasing the efficiency. The photocatalytic behavior of $TiO_2@ZnIn_2S_4$ and $CuO/ZnIn_2S_4$ composites for the degradation of MB under visible light irradiation were investigated, demonstrating that the photocatalytic activity of $ZnIn_2S_4$ could be greatly enhanced by modification with TiO_2 and CuO. In addition, the possible mechanisms for the enhanced photocatalytic activity of $TiO_2@ZnIn_2S_4$ and $CuO/ZnIn_2S_4$ photocatalysts for MB degradation were proposed.

Experimental

Synthesis of TiO_2@$ZnIn_2S_4$ composite [28]

The core-shell TiO_2@$ZnIn_2S_4$ composite samples were synthesized via a hydrothermal process. All chemicals were analytical grade and used as received without further purification. In a typical reaction, a certain amount of TiO_2 was dispersed uniformly by ultrasonication in 60 mL deionized water, $ZnCl_2$ (1 mmol) and $In(NO_3)_3 \cdot 4.5H_2O$ (2 mmol) were added in a stoichiometric ratio, and then excessive thioacetamide (TAA, 6 mmol) was dissolved in the system. The mixed solution was then transferred to a 200 mL Teflon-lined autoclave. The autoclave was sealed, kept at 160 °C for 6 h, and then naturally cooled down to room temperature. The precipitates were filtered and washed with distilled water and absolute ethanol several times. The obtained samples were dried in a vacuum at 80 °C for 6 h. As a control, $ZnIn_2S_4$ powders were synthesized under similar conditions without adding TiO_2.

Synthesis of CuO/$ZnIn_2S_4$ composites

CuO/$ZnIn_2S_4$ photocatalyst was prepared by the impregnation-calcination method with $ZnIn_2S_4$ as precursor. All chemicals were analytical grade and used as received without further purification. The desired amount $ZnIn_2S_4$ powder was added into various concentration of copper nitrate solution, followed by ultrasonic process to get homogeneous slurry. After wet impregnation, the sample was dried at 65 °C overnight. The dried sample was then washed with distilled water several times to remove unbound copper, and finally calcined in air at 300 °C for 4 h [29]. Considering the structure, morphology, and photocatalytic activity of photocatalysts are affected by reactant concentration, calcination temperature [30]. A series of CuO/$ZnIn_2S_4$ composites were prepared by changing the concentration of the copper

nitrate solution in the preparation procedure. The as-prepared $CuO/ZnIn_2S_4$ composites are designated as x mol% $CuO/ZnIn_2S_4$ (x=0, 5, 7, 10, 15, 20), mol% = $n_{Cu}/(n_{Cu} + n_{ZnIn_2S_4})$, respectively.

Characterization of materials

X-ray diffraction (XRD) patterns were obtained by Bruker D8 Advance X-ray diffractometer with Cu-Kα irradiation (λ = 1.54 Å) at 40 kV and 40 mA. The general morphology of the products was examined by scanning electron microscopy (SEM) on a JEOL JSM 6700 F instrument operated at 20 kV. The transmission electron microscopy (TEM) images were measured by JEOL model JEM 2010 EX instrument at the accelerating voltage of 200 kV. The specific surface area and porosity of the samples were measured by N_2 adsorption at 77 K on a Micrometritics ASAP2020 analyzer and calculated by the Brunauer-Emmett-Teller (BET) method. All of the samples were degassed at 120 °C overnight prior to BET measurements. The UV-Vis diffuse reflectance spectra (DRS) were conducted with a Varian Cary 500 UV-Vis spectrophotometer with $BaSO_4$ as the reference.

Photocatalytic activity measurement

The photocatalytic activities of all powders were evaluated by degradation of MB aqueous solution. The visible light was obtained by a 250 W tungsten-halogen lamp with a 420 nm cut off filter. A suspension containing 20 mg of catalyst and a fresh MB aqueous solution (120 mL, 20 mg/L) was magnetically stirred in the dark for 1 h to establish an adsorption/desorption equilibrium. At certain time intervals, 3~4 mL of suspension was sampled and the particles were removed. The filtrate was

analyzed by a UV-Vis spectrophotometer (UV-2450) and the absorption peaks at maximum absorption wavelength (665 nm) for MB were monitored.

Results and discussion

Phase structure

Fig. 1 shows XRD patterns of (a) TiO_2, (b) TiO_2@$ZnIn_2S_4$ composite, (c) $ZnIn_2S_4$. As can be seen, the naked $ZnIn_2S_4$ displays diffraction peaks of (006), (102), (112), (1012) and (202) crystal planes at 2θ = 21.68, 27.88, 47.28, 52.18 and 56.18, which can be indexed to a hexagonal phase of $ZnIn_2S_4$ (JCPDS No. 65-2023) [31]. The XRD pattern of TiO_2@$ZnIn_2S_4$ composite is very similar to the naked $ZnIn_2S_4$ and TiO_2. All diffraction peaks of $ZnIn_2S_4$ are still present in the XRD pattern of TiO_2@$ZnIn_2S_4$ composite, indicating that $ZnIn_2S_4$ sample was not destroyed during the synthesis process after TiO_2 addition. These findings were in agreement with previous report [32] and confirmed that the TiO_2/ $ZnIn_2S_4$ composite sample was successfully prepared.

Fig. 1 also shows the XRD patterns of CuO/$ZnIn_2S_4$ photocatalysts with different CuO content. When CuO content was lower than 7 mol%, no characteristic peaks of either metallic copper or copper oxide were detected, which may be explained by the small amount of Cu species content and highly dispersion in the samples, which were beyond the detection limit of the XRD technique. At higher CuO content, characteristic peaks of CuO crystal (2θ = 35.5°, 38.7°) [22] can be observed, their intensities are enhanced with increasing the CuO content, indicating the existence of CuO. The XRD results clearly show no presence of other copper species (i.e. Cu_2O)) and impurity phases, indicating that all samples have a high crystallinity. The spectra

of the composite catalysts did not change much when the loading amount of CuO increasing from 5 mol% to 20 mol%.

As also clearly shown from the XRD patterns above, for all photocatalyst composites, characteristic peaks of $ZnIn_2S_4$ are observed, and there are no significant changes of intensities. It indicates that $ZnIn_2S_4$ had scarcely undergone phase transformation and particle size change during the preparation process. The same crystal structure of $ZnIn_2S_4$ in different composite samples can generate a similar amount of photo-induced electrons and holes. As a result, the unchanged crystal structure of $ZnIn_2S_4$ did not contribute to the improvement of the photocatalytic activity.

Morphological structure

The specific structure and size of the as-synthesized TiO_2@$ZnIn_2S_4$ composite photocatalysts were examined by transmission electron microscopy (TEM). Fig. 2(a) [28] presents an individual microspherical particle with a zigzag circle and with a diameter about 270 nm. The TEM image (Fig. 2b) [28] reveals that TiO_2@$ZnIn_2S_4$ nanoparticles are composed of a unique core-shell structure with a distinct dark outer layer ($ZnIn_2S_4$; approximately 20-30 nm thickness) and a gray inner region (TiO_2), clearly demonstrating the formation of core-shell structure. The corresponding TEM image (Fig. 2c) reveals the well-defined core-shell structures of TiO_2@$ZnIn_2S_4$. The core of TiO_2 composites is entirely coated and connected with $ZnIn_2S_4$ shell, confirming the formation of heterojunctions between TiO_2 and $ZnIn_2S_4$ through the hydrothermal process and the intimate contact between TiO_2 and $ZnIn_2S_4$. It has been confirmed that the $ZnIn_2S_4$ shells have been deposited over the TiO_2 cores in the TiO_2@$ZnIn_2S_4$ sample, and TiO_2 was evenly capped with $ZnIn_2S_4$.

The morphologies of $CuO/ZnIn_2S_4$ photocatalysts with different CuO content were observed by SEM measurement (Fig. 3). It can be see clearly that the introduction of CuO directly affects the morphology of $CuO/ZnIn_2S_4$. In the absence of CuO, $ZnIn_2S_4$ sample exhibits a lot of separate microspheres with the diameter of 1-3 μm, as shown in Fig. 3a. Further observation shows that all the microspheres are composed of numerous petals/sheets. This growth tendency of lamellar structures might be related to the layered feature of hexagonal $ZnIn_2S_4$. When the CuO content was increased from 5 mol% to 10 mol%, $ZnIn_2S_4$ products still presented to be microspheres, while the diameter of $CuO/ZnIn_2S_4$ microspheres decreased gradually. As CuO content increased further, the shape of microspheres for $CuO/ZnIn_2S_4$ was destructed partially and even throughly, as shown in Fig. 3e-f, as well as the petals/sheets presented to be more irregular. Obviously, instead of microspheres and petals/sheets, $CuO/ZnIn_2S_4$ turned out to be a bulky aggregation with a rough surface, and petals/sheets could be hardly observed when the CuO content was up to 15~20 mol%. In summary, compared to $ZnIn_2S_4$, the $CuO/ZnIn_2S_4$ composites showed less uniform morphology and particle size distribution, inclining to connect together after coupling with CuO so that the edges of $ZnIn_2S_4$ got fuzzy and irregular. The interconnected structure for $CuO/ZnIn_2S_4$ composites made the interfacial charge transfer available between CuO and $ZnIn_2S_4$, which could be expected to play an important role in promoting the photocatalytic activities of the resulting $CuO/ZnIn_2S_4$ composite photocatalysts.

Optical properties

Fig. 4 [28] illustrates the UV-vis diffuse reflectance absorption spectra (DRS) of $ZnIn_2S_4$, TiO_2 and $TiO_2@ZnIn_2S_4$ composite. TiO_2 can only be excited by light of short wavelengths ($\lambda \leq 387$ nm), leading to low efficiency for utilizing solar energy

[33]. The spectrum of TiO_2 consists of a single absorption below ca. 370 nm usually ascribed to charge transfer from the valence band (mainly formed by 2p orbitals of the oxide anions) to the conduction band (mainly formed by $3d_{t2g}$ orbitals of the Ti^{4+} cations), suggesting TiO_2 has no photocatalytic activity under visible light irradiation. The TiO_2@$ZnIn_2S_4$ heterostructures composite showed an additional transition, with the absorption from 400 to 500 nm. We believe that a partial interfacial charge transfer between $ZnIn_2S_4$ and TiO_2 was probably responsible for this diminished absorption because such a transition cannot be assigned to the synergistic effect of the two components. This spectrum demonstrated that TiO_2 addition had a slight effect on the absorption properties of $ZnIn_2S_4$, since the TiO_2@$ZnIn_2S_4$ hybridization photocatalyst didn't exactly expand its photo-response to visible region in comparison with pristine $ZnIn_2S_4$.

Fig. 5 shows the UV-Vis diffuse reflectance spectra of CuO/$ZnIn_2S_4$ composites. There was a significant enhancement of absorption in visible light region at (420 to 700 nm) with the loading of CuO. Such additional broad band can be assigned to the absorption of CuO, coupling interaction between the CuO and $ZnIn_2S_4$ phase, the optimizing loading amount of CuO and the form of heterojunction structure at the same time, which leads to the enhancement of utilization of light and photocatalytic activity. The visible light responses of the CuO/$ZnIn_2S_4$ samples are significantly improved and will be easier to generate electron-hole pairs, which will result in higher photocatalytic activities of $ZnIn_2S_4$. The visible light absorption intensity of CuO/$ZnIn_2S_4$ increased initially with increasing CuO concentration, and then decreased as the CuO concentration further increased. The results indicated that the visible-light-response of 10 mol% CuO/$ZnIn_2S_4$ composite photocatalyst was greatly improved by coupling the appropriate amount of CuO. Therefore, 10 mol%

$CuO/ZnIn_2S_4$ composite photocatalyst exhibited the higher photocatalytic efficiency than others. This phenomenon was similar to the investigation of the deposition CdS nanocrystals on TiO_2 films [34]. A "shading effect", in which colored CuO absorbed light and reduced the photoexciting capacity of $ZnIn_2S_4$, was invoked to explain the detrimental effect of CuO loading beyond the optimum.

For both coupled heretostructure composites, pure $ZnIn_2S_4$ sample shows a wide absorption in visible region with an absorption edge end at about 580 nm, corresponding to the band gap of 2.14 eV according to the Tauc equation. All of the samples show the strong absorption in the visible light regions. The steep shape of the spectrum indicates that the visible light absorption is not due to the transition from the impurity level but due to the band gap transition [35-36].

Photocatalytic properties

The visible light photocatalytic activity of the all samples was evaluated with the photodegradation of MB in aqueous solution. As shown in Fig. 6, in the presence of TiO_2, the concentration of MB essentially remained constant, that is to say, the TiO_2 paticles played no role in degrading MB under visible light irradiation, since TiO_2 cannot be excited by visible light irradiation which is consistent with the change tendency of the DRS spectrum. The result demonstrated that TiO_2 has no photocatalytic activity under visible light irradiation. On the contrary, about 71% of MB was degraded after 3 h of irradiation with pure $ZnIn_2S_4$, compared to nearly 90% degradation of MB with $TiO_2@ZnIn_2S_4$ composite, which also exhibited more efficient photocatalytic activity. As we know, the light absorption capability of photocatalyst and separation of excited electron-hole pairs are the two crucial factors influencing the photoactivity. Based on the DRS results, the absorption ability of the

TiO_2@$ZnIn_2S_4$ sample did not significantly contribute to the photocatalytic activity of the as-prepared sample compared with that of pure $ZnIn_2S_4$. In other words, the main role of TiO_2 is an electron acceptor that suppresses electron-hole recombination in $ZnIn_2S_4$. Meanwhile, because $ZnIn_2S_4$ nanosheets are uniformly grown on the surface of TiO_2, excessive aggregation of $ZnIn_2S_4$ can be avoided, which will increase reaction active sites and reactant adsorption. The strong coupling effect between $ZnIn_2S_4$ and TiO_2 is awfully important for the photogenerated charge transfer. At the same time, the intimate contact between TiO_2 and $ZnIn_2S_4$ favors the formation of junctions between the two components [37]. In result, core-shell TiO_2@$ZnIn_2S_4$ composites exhibited significantly enhanced the photocatalytic activity, highlighting the usefulness of the combination with TiO_2 in improving the photocatalytic activity of the $ZnIn_2S_4$ nanosheets through fast electron transfer between two conduction bands.

As shown in Fig. 7, the photocatalytic activity of CuO/$ZnIn_2S_4$ products with different CuO content exhibited markedly higher photocatalytic activity than that of pure $ZnIn_2S_4$ under visible light irradiation. With the increase of CuO content, the photocatalytic activity of CuO/$ZnIn_2S_4$ experienced a rise first followed by a decline which means excess CuO had a negative effect on catalytic activity, revealing there was an appropriate ratio between CuO and $ZnIn_2S_4$ in this kind of composites. The highest photocatalytic activity was obtained by the 10 mol% CuO/$ZnIn_2S_4$ composite, with a MB decoloration of 97% within 3 h. The initial increased CuO particles can play dual roles in enhancing photocatalytic activity by increasing visible light absorption and acting as reduction sites for MB degradation. The following regression of photocatalytic activity observed with the loading amount of CuO increasing from 15 mol% to 20 mol% may be due to the fact that excess CuO particles loaded on the

surface of $CuO/ZnIn_2S_4$ could act as the optical filter or charge recombination center instead of co-catalyst for charge separation [14], though the visible-light absorption band grew further. Such a similar dependence of photocatalytic performance upon the amount of loading has been observed for several other photocatalysts [16, 32, 38]. These results indicate that the photocatalytic activites depend upon not only the visible-light absorption (i.e., band gap) but also some other factors. In this study, the existence of CuO is much favorable to enhance the photocatalytic activities of the samples and the improvement of photocatalytic performances of $CuO/ZnIn_2S_4$ represented the synergy effect. At higher CuO content, a part of photocatalyst particles would be encapsulated completely by CuO particles, resulting in a notable decrease of the activity [39]. It is worth noting that there are two factors that limited performance at high CuO loading: (1) blockage of active sites by excess amounts of CuO introduced in the photocatalysts and (2) an increase in opacity and light scattering of $CuO/ZnIn_2S_4$ at a high concentration leads to a decrease in the passage of light through the sample.

To evaluate the stability of the photocatalytic performance of the $TiO_2@ZnIn_2S_4$ and $CuO/ZnIn_2S_4$ heterostructure catalysts, which is an important factor in practical application in environmental remediation, the circulating runs of the photocatalytic degradation of MB were studied under visible light irradiation (Fig. 8). It is noted that the $TiO_2@ZnIn_2S_4$ and $CuO/ZnIn_2S_4$ photocatalysts are easily recycled by simple filtration. After five cycles, the photocatalytic activity of both composites exhibit no obvious loss for degradation of MB, confirming that the components of the $TiO_2@ZnIn_2S_4$ and $CuO/ZnIn_2S_4$ heterostructure are not photocorroded and the heterojunction structure is stable during the photocatalytic process. In addition, a significant enhancement is observed in the photocatalytic degradation of MB for

$CuO/ZnIn_2S_4$ contact type heterostructure composites compared with $TiO_2@ZnIn_2S_4$ core-shell type heterostructure composites, which may be attributed to the fact that the former exhibits great potential for extending the light absorption range of semiconductors besides facilities charge separation and transfer unlike the latter is only of benefit to charge separation and transfer.

BET Surface Area Analyses

To investigate the effects of CuO addition on the BET specific surface area of $ZnIn_2S_4$ photocatalysts, the nitrogen adsorption-desorption isotherms of the samples were further investigated. Fig. 9 shows the liquid nitrogen adsorption-desorption isotherm of $ZnIn_2S_4$ prepared at 160 °C with corresponding pore size distribution (BJH method, inset). The nitrogen adsorption and desorption isotherms are identified as type IV isotherm with a hysteresis loop and the pore size distribution plot reveals that the diameter of the product is about 2-40 nm, indicating the presence of mesoporous structure in the products. As expected, the BET surface area of the composites decreased as the CuO content increased, as shown in Table 1. The decrease in BET specific surface area of $CuO/ZnIn_2S_4$ was attributed to the blockage of $ZnIn_2S_4$ channel caused by CuO during the impregnation-calcination process. This result was also in accordance with the observation of SEM images because of the formation of imperfect microspheres, petals/sheets structure after CuO loaded. In general, the BET surface of a photocatalyst can greatly affect its photocatalytic performance. A high BET surface area corresponds to the good photocatalytic activity [40-41]. Nevertheless, the relatively smaller surface area for the samples than that of pristine $ZnIn_2S_4$ could not be the decisive factor for its high activity.

As is well known, adsorption ability, phase structure and separation efficiency of photogenerated charges are crucial factors for photocatalytic activity [42]. BET and adsorption experiments were performed to investigate the adsorption ability of $ZnIn_2S_4$ and $CuO/ZnIn_2S_4$. Compared with that of pure $ZnIn_2S_4$, $CuO/ZnIn_2S_4$ shows an enhanced adsorptivity. As discussed above, the phase structure of $ZnIn_2S_4$ remain unchanged and adsorptivity of $ZnIn_2S_4$ enhances a little, we believe that the enhancement of the photocatalytic activity of the $CuO/ZnIn_2S_4$ photocatalysts is attributed mainly to the effective separation of the photogenerated electron-hole pairs and the small differences of the surface areas suggest that the surface area is not a decisive factor for the photocatalytic activities.

Mechanisms of photocatalysis

On the basis of the above experimental results and discussion, the expected working mechanisms for photocatalytic over the hierarchical core-shell $TiO_2@ZnIn_2S_4$ and $CuO/ZnIn_2S_4$ composites under visible-light irradiation are shown in Fig. 10. Under visible light irradiation, for $TiO_2@ZnIn_2S_4$ core-shell type heterostructure composites, TiO_2 shows no photoelectronic response, whereas $ZnIn_2S_4$ is excited and yields photogenerated electrons from the valence band (VB) to its conduction band (CB). At the interface of coupled TiO_2 and $ZnIn_2S_4$ core-shell heterojunction in which TiO_2 act as the electron acceptor, the Fermi level of TiO_2 and $ZnIn_2S_4$ will align in equilibrium. The potential of conduction band edge of $ZnIn_2S_4$ is 1.18 eV [43]. So the photogenerated electrons can transfer from CB of $ZnIn_2S_4$ to that of TiO_2 driven by the action of built-in electric field and the concentration gradient, while the holes accumulate in VB of $ZnIn_2S_4$ due to the lower voltage forbidden. However, for $CuO/ZnIn_2S_4$ contact type heterostructure composites, $ZnIn_2S_4$ and CuO are excited simultaneously and electron-hole pairs are generated. Because the CB

edge of $ZnIn_2S_4$ is more negative than that of CuO, electrons in CB of $ZnIn_2S_4$ easily flow to the CB edge of CuO through the interface. On the other hand, holes in the VB edge of CuO will transfer to that of $ZnIn_2S_4$ because the VB edge level of CuO is more positive than that of $ZnIn_2S_4$. The photogenerated electrons and holes are thus effectively separated at the $ZnIn_2S_4$/CuO interface and then migrate to the surface of the catalyst. Through this separation progress, the recombination of photogenerated electrons and holes is inhibited to a certain extent in both type heterostructure composites. Then, the photogenerated electrons will then be captured by O_2 to yield $\cdot O_2^-$, and finally form ·OH [44]. ·OH will further oxidize the MB molecules to form CO_2 and H_2O completely. On the other hand, the photoinduced holes in $ZnIn_2S_4$ are powerful oxidative species, which will oxidize MB directly, leading to its decomposition [45]. Therefore, these will decrease the recombination rate of the electron-hole pairs in all samples, resulting in the enhancement of photocatalytic efficiency.

The excellent performance of the core-shell TiO_2@$ZnIn_2S_4$ composites can be ascribed to several factors: (1) fast separation of the photoinduced electron/hole pairs plays an important role; (2) The intimate contact and formation of junctions between $ZnIn_2S_4$ and TiO_2 could offer effective charge separation; (3) TiO_2 in the hierarchical structure composites acts as the electron acceptor and makes electron transport excellent.

The introduction of CuO into $ZnIn_2S_4$ results in better harvest of incident light. Obviously, the improved photocatalytic efficiency of the CuO/$ZnIn_2S_4$ photocatalysts can be attributed to the synergistic effect of the two components. With increasing of CuO loading amount, this synergistic effect is positive for enhancing photocatalytic activity, but at higher loading amount the excess CuO may cover active sites resulting

a reduction of photon absorption and act as a recombination sites for charges [46] on $ZnIn_2S_4$ surface.

Conclusions

The charge separation and photocatalytic activities were enhanced by selectively coupling/modifying $ZnIn_2S_4$ with TiO_2 and CuO semiconductors through forming heterostructure composites compared to $ZnIn_2S_4$. For TiO_2@$ZnIn_2S_4$ heterostructure composites, the core-shell structure plays a crucial role. While for CuO/$ZnIn_2S_4$ heterostructure composites, it may be attributed to the enhanced separation of photo-generated electrons and holes induced by the hybridization of $ZnIn_2S_4$ with CuO and expand its photo-response to visible region through formation of impurity energy levels. The as-prepared composite showed the highest photocatalytic activity for MB dye wastewater treatment by coupling 10 mol% CuO. It is worth emphasizing that excess CuO could cover the activity centers of the catalysts and reduce the light absorption. The effectively integrated structure and the electronic properties of the CuO/$ZnIn_2S_4$ are essential for a high active photocatalyst.

Acknowledgments

The authors gratefully acknowledge the financial support of National Natural Science Foundation of China (No.20976057) and research fund of The Guangdong Provincial Engineering Research Centre of Green Fine Chemicals, China.

Notes and references

[a]*School of Chemistry and Chemical Engineering, South China University of Technology, Guangdong Guangzhou 510640; Tel: +86 20 8711 1887; fax: +86 20 8711 1887. E-mail address: cewhyuan@scut.edu.cn; Present Address: School*

of Chemistry and Chemical Engineering, South China University of Technology, Wushan, Tianhe, Guangzhou 510640, P. R. China.

[b]*College of Environmental Science and Engineering, South China University of Technology, Guangdong Guangzhou 510006*

Electronic Supplementary Information (ESI) available: **Figure SI 1.** XRD patterns of (a) TiO_2, (b) TiO_2@$ZnIn_2S_4$, (c) $ZnIn_2S_4$, (d) 5 mol% CuO/$ZnIn_2S_4$, (e) 7 mol% CuO/$ZnIn_2S_4$, (f) 10 mol% CuO/$ZnIn_2S_4$, (g) 15 mol% CuO/$ZnIn_2S_4$, (h) 20 mol% CuO/$ZnIn_2S_4$. **Figure SI 2.** TEM images of (a) $ZnIn_2S_4$ and (b), (c) TiO_2@$ZnIn_2S_4$ composite. **Figure SI 3.** SEM images of CuO/$ZnIn_2S_4$ with variation of CuO content (a) 0, (b) 5 mol%, (c) 7 mol%, (d) 10 mol%, (e) 15 mol%, (f) 20 mol%. **Figure SI 4.** UV-vis absorption property of $ZnIn_2S_4$, TiO_2 and TiO_2@$ZnIn_2S_4$ composite. **Figure SI 5.** UV-vis absorption property of the CuO/$ZnIn_2S_4$ products with variation of CuO content (a) 0, (b) 5 mol%, (c) 7 mol%, (d) 10 mol%, (e) 15 mol%, (f) 20 mol%. **Figure SI 6.** Photocatalytic degradation of MB over $ZnIn_2S_4$, TiO_2 and TiO_2@$ZnIn_2S_4$ composite. **Figure SI 7.** Photocatalytic degradation of MB over the CuO/$ZnIn_2S_4$ products with variation of CuO content (a) 0, (b) 5 mol%, (c) 7 mol%, (d) 10 mol%, (e) 15 mol%, (f) 20 mol%. **Figure SI 8**. Recyclability tests of TiO_2@$ZnIn_2S_4$ (3 h), 10 mol% CuO/$ZnIn_2S_4$ (3 h) photocatalyst for degradation of MB under visible light irradiation. **Figure SI 9.** Nitrogen adsorption-desorption isotherms and the pore size distribution plot (inset) of $ZnIn_2S_4$. **Figure SI 10.** Band structures model of coupled-photocatalysts in core-shell type heterostructure composites and contact type heterostructure composites.

[1] T.A. Gad-Allah, K. Fujimura, S. Kato, S. Satokawa, T. Kojima, J. Hazard. Mater., 2008, **154**, 572-577.

[2] M.A. Gondal, X.F. Chang, Z.H. Yamani, Chem. Eng. J., 2010, **165**, 250-257.

[3] M. Sun, D.Z. Li, W.J. Zhang, Z.X. Chen, H.J. Huang, W.J. Li, Y.H. He, X.Z. Fu, J. Solid State Chem., 2012, **190**, 135-142.

[4] T.Y. Peng, D.N. Ke, J.R. Xiao, L. Wang, J. Hu, L. Zan, J. Solid State Chem., 2012, **194**, 250-256.

[5] G. Patrinoiu, M. Tudose, J.M. Calderon-Moreno, R. Birjega, P. Budrugeac, R. Ene, O. Carp, J. Solid State Chem., 2012, **186**, 17-22.

[6] D. Chen, D. Yang, Q. Wang, Z. Jiang, Ind. Eng. Chem. Res., 2006, **45**, 4110-4116.

[7] H. Liu, X.N. Dong, G.J. Li, X. Su, Z.F. Zhu, Appl. Surf. Sci., 2013, **271**, 276-283.

[8] S.L. Bai, H.Y. Li, Y.J. Guan, S.T. Jiang, Appl. Surf. Sci., 2011, **257**, 6406-6409.

[9] A.V. Borhade, D.R. Tope, B.K. Uphade, E-J. Chem., 2012, **9**, 705-715.

[10] Z.D. Xu, Y.X. Li, S.Q. Peng, G.X. Lu, S.B. Li, RSC Adv., 2012, **2**, 3458-3466.

[11] Z.D. Xu, Y.X. Li, S.Q. Peng, G.X. Lu, S.B. Li, CrystEngComm, 2011, **13**, 4770-4776.

[12] L.M. Wu, F. Fang, L. Chen, Y.B. Chen, J. Phys. Chem. C, 2010, **114**, 2393-2397.

[13] S.H. Shen, L. Zhao, L.J. Guo, Int. J. Hydrogen Energy, 2008, **33**, 4501-4510.

[14] S.H. Shen, L. Zhao, Z. Zhou, J. Phys. Chem. C, 2008, **112**, 16148-16155.

[15] W.H. Yuan, X.C. Liu, L. Li, Acta Phys. Chim. Sin., 2013, **29**, 151-156.

[16] B. Chai, T.Y. Peng, P. Zeng, X.H. Zhang, Dalton Trans., 2012, **41**, 1179-1186.

[17] Y.G. Yu, G. Chen, G. Wang, Z.S. Lv, Int. J. Hydrogen Energy, 2012, **38**, 1278-1285.

[18] V.V. Bozhko, A.V. Novosad, G.E. Davidyuk, V.R. Kozer, O.V. Parasyuk, N. Vainorius, V. Janonis, A. Sakavicius, V. Kazukauskas, J. Alloys Compd., 2013, **553**, 48-52.

[19] Z.W. Mei, S.X. Ouyang, D.M. Tang, T. Kako, D. Golberg, J.H. Ye, Dalton Trans., 2013, **42**, 2687-2690.

[20] J. Zhou, G.H. Tian, Y.J. Chen, X.Y. Meng, Y.H. Shi, X.R. Cao, K. Pan, H.G. Fu, Chem. Commun., 2013, **49**, 2237-2239.

[21] X. Zong, G.P. Wu, H.J. Yan, G.J. Ma, J.Y. Shi, F.Y. Wen, L. Wang, C. Li, J. Phys. Chem. C, 2010, **114**, 1963-1968.

[22] S.P. Xu, D.D. Sun, Int. J. Hydrogen Energy, 2009, **34**, 6096-6104.

[23] Z.L. Jin, X.J. Zhang, Y.X. Li, S.B. Li, G.X. Lu, Cataly. Commun., 2007, **8**, 1267-1273.

[24] H. Widiyandari, A. Purwanto, R. Balgis, T. Ogi, K. Okuyama, Chem. Eng. J., 2012, **180**, 323-329.

[25] C.K. Ngaw, Q.C. Xu, T.T.Y. Tan, P. Hu, S.W. Cao, J.S.C. Loo, Chem. Eng. J., 2014, **257**, 112-121.

[26] Y.B. Li, Z.F. Liu, Y. Wang, Z.C. Liu, J.H. Han, J. Ya, Int. J. Hydrogen Energy, 2012, **37**, 15029-15037.

[27] G.H. He, G.L. He, A.J. Li, X. Li, X.J. Wang, Y.P. Fang, Y.H. Xu, J. Mol. Catal. A-Chem., 2014, **385**, 106-111.

[28] W.H. Yuan, Z.L. Xia, L. Li, Chin. Chem. Lett., 2013, **24**, 984-986.

[29] J. Bandara, C.P.K. Udawatta, C.S.K. Rajapakse, Photochem. Photobiol., 2005, **4**, 857-861.

[30] W.H. Yuan, X.X. Liu, L. Li, Appl. Surf .Sci., 2014, **7**, 28405-28413.

[31] Z.X. Chen, D.Z. Li, W.J. Zhang, J. Phys. Chem. C, 2009, **113**, 4433-4440.

[32] S.J. Peng, Y.Z. Wu, P.N. Zhu, J. Mater. Chem., 2011, **21**, 15718-15726.

[33] S.Q. Peng, Y.H. Huang, Y.X. Li, Mat. Sci. Semicon. Proc., 2013, **16**, 62-69.

[34] C.H. Chang, Y.L. Lee, Appl. Phys. Lett., 2007, **91**, 53503-53505.

[35] L. Zhou, W. Wang, L. Zhang, H.L. Xu, W. Zhu, J. Phys. Chem. C, 2007, **111**, 13659-13664.

[36] Y.X. Li, K. Zhang, S.Q. Peng, G.X. Lu, S.B. Li, J. Mol. Catal. A-Chem., 2012, **363-364**, 354-361.

[37] X. Zong, H.J. Yan, G.P. Wu, J. Am. Chem. Soc., 2008, **130**, 7176-7177.

[38] A.J. Simamora, T.L. Hsiung, F.C. Chang, T.C. Yang, C.Y. Liao, Int. J. Hydrogen Energy, 2012, **37**, 13855-13858.

[39] Y.X. Li , S.Y. Lin , S.Q. Peng , G.X. Lu , S.B. Li, Int. J. Hydrogen Energy, 2013, **38**, 15976-15984.

[40] L.S. Zhang, W.Z. Wang, Z.G. Chen, L. Zhou, H.L. Xu, W. Zhu, J. Mater. Chem., 2007, **17**, 2526-2532.

[41] M. Shang, W.Z. Wang, J. Ren, S.M. Sun, L. Zhang, CrystEngComm, 2010, **12**, 1754-1758.

[42] L.W. Zhang, H.B. Fu and Y.F. Zhu, Adv. Funct. Mater., 2008, **18**, 2180-2189.

[43] Y.X. Li, J.X. Wang, S.Q. Peng, G.X. Lu, S.B. Li, Int. J. Hydrogen Energy, 2010, **35**, 7116-7126.

[44] N. Wetchakun, S. Chaiwichain, B. Inceesungvorn, K. Pingmuang, S. Phanichphant, A.I. Minett, J. Chen, ACS Appl. Mater. Interfaces, 2012, **4**, 3718-3723.

[45] P. Ju, P. Wang, B. Li, H. Fan, S.Y. Ai, D. Zhang, Y. Wang, Chem. Eng. J., 2014, **236**, 430-437.

[46] H. Xu, H.M. Li, C.D. Wu, J.Y. Chu, Y.S. Yan, H.M. Shu, Z. Gu, J. Hazard. Mater., 2008, **153**, 877-884.

Figures

Fig. 1. XRD patterns of (a) TiO_2, (b) TiO_2@$ZnIn_2S_4$, (c) $ZnIn_2S_4$, (d) 5 mol% CuO/$ZnIn_2S_4$, (e) 7 mol% CuO/$ZnIn_2S_4$, (f) 10 mol% CuO/$ZnIn_2S_4$, (g) 15 mol% CuO/$ZnIn_2S_4$, (h) 20 mol% CuO/$ZnIn_2S_4$.

Fig. 2. TEM images of (a) $ZnIn_2S_4$ and (b), (c) TiO_2@$ZnIn_2S_4$ composite.

Fig. 3. SEM images of CuO/$ZnIn_2S_4$ with variation of CuO content (a) 0, (b) 5 mol%, (c) 7 mol%, (d) 10 mol%, (e) 15 mol%, (f) 20 mol%.

Fig. 4. Diffuse reflectance spectra (DRS) of $ZnIn_2S_4$, TiO_2 and TiO_2@$ZnIn_2S_4$ composite.

Fig. 5. Diffuse reflectance spectras of CuO/$ZnIn_2S_4$ with variation of CuO content (a) 0, (b) 5 mol%, (c) 7 mol%, (d) 10 mol%, (e) 15 mol%, (f) 20 mol%.

Fig. 6. Visible-light photocatalytic activity of $ZnIn_2S_4$, TiO_2 and TiO_2@$ZnIn_2S_4$ composite.

Fig. 7. Visible-light photocatalytic activity of the CuO/$ZnIn_2S_4$ products with variation of CuO content (a) 0, (b) 5 mol%, (c) 7 mol%, (d) 10 mol%, (e) 15 mol%, (f) 20 mol%.

Fig. 8. Recyclability tests of (a) TiO_2@$ZnIn_2S_4$ (3 h), (b) 10 mol% CuO/$ZnIn_2S_4$ (3 h) photocatalyst for degradation of MB under visible light irradiation.

Fig. 9. Nitrogen adsorption-desorption isotherms and the pore size distribution plot (inset) of $ZnIn_2S_4$.

Fig. 10. Band structures model of coupled-photocatalysts in core-shell type heterostructure composites and contact type heterostructure composites.

Fig. 1

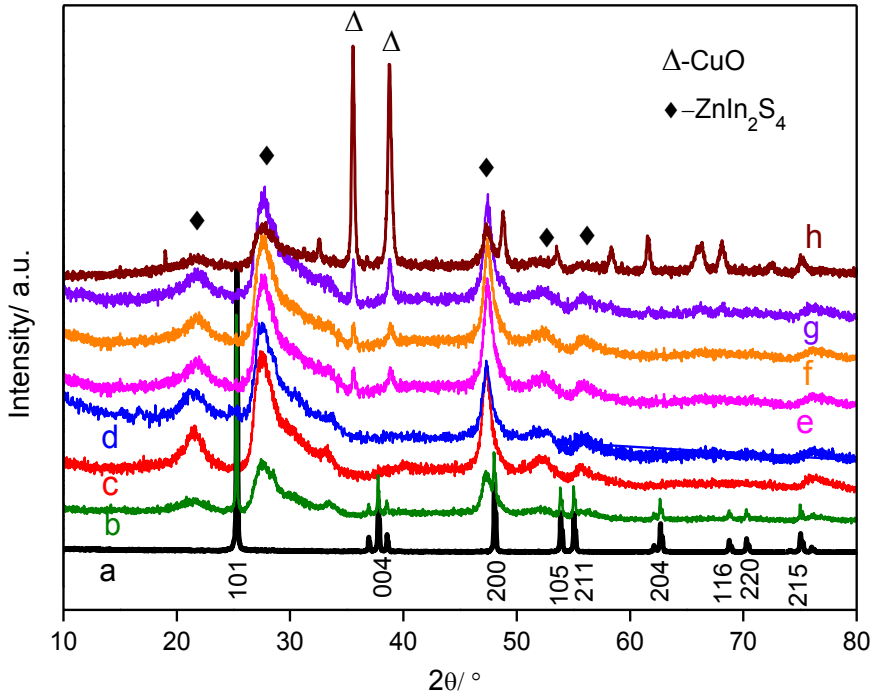

Fig. 2

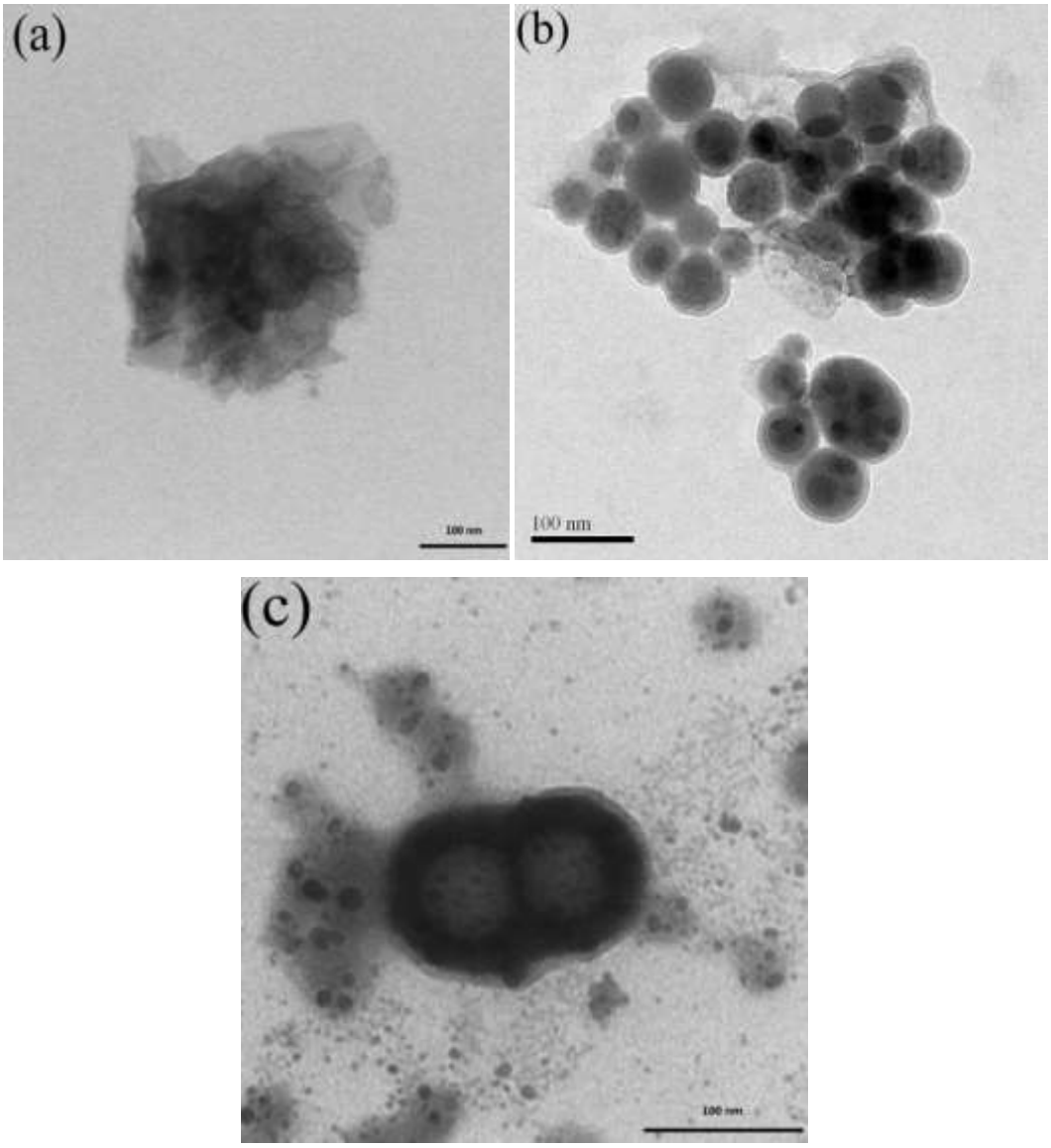

Fig. 3

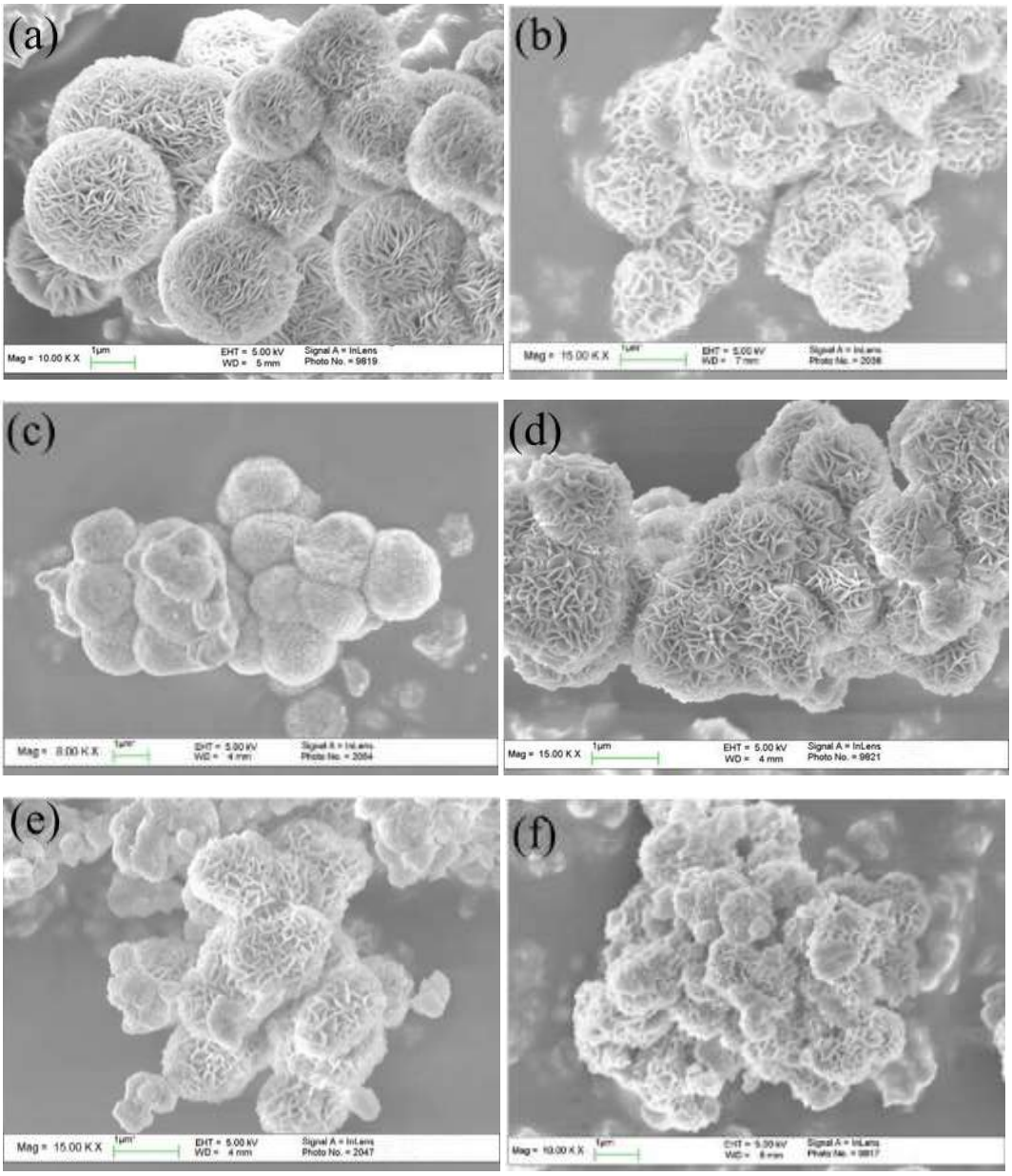

Fig. 4

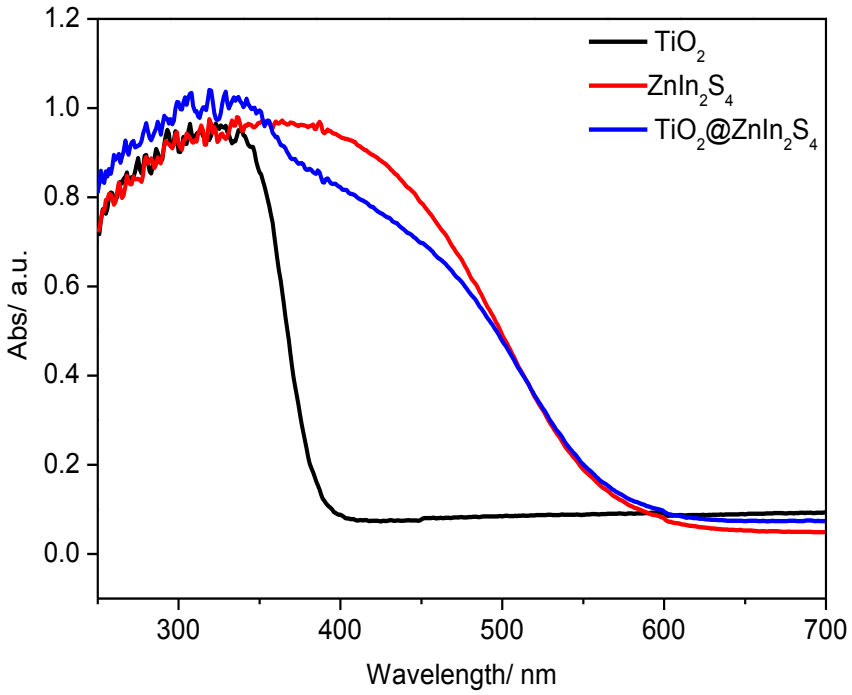

Fig.5

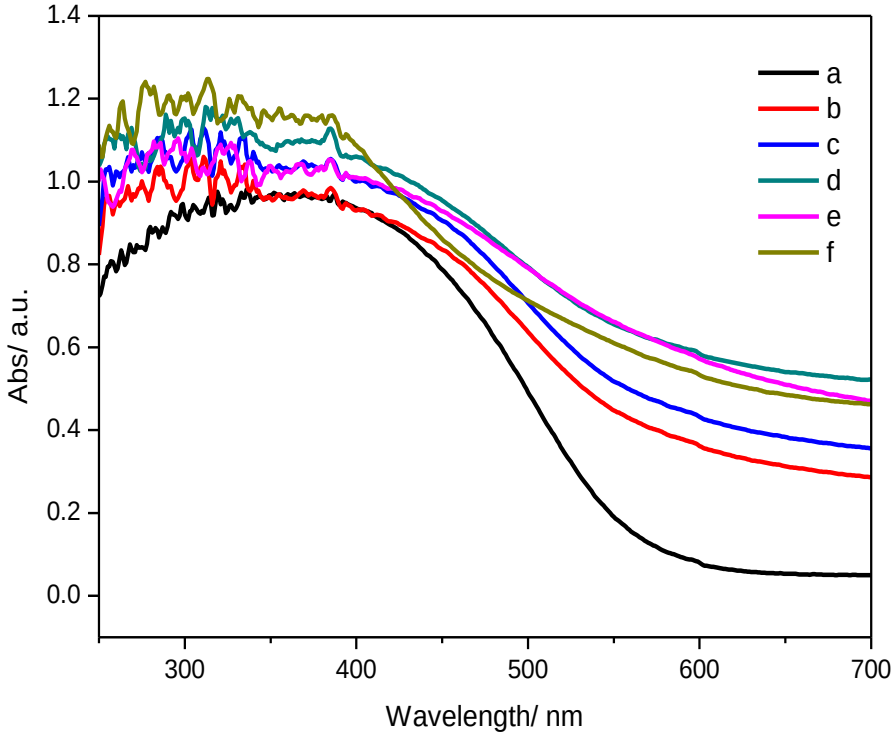

Fig.6

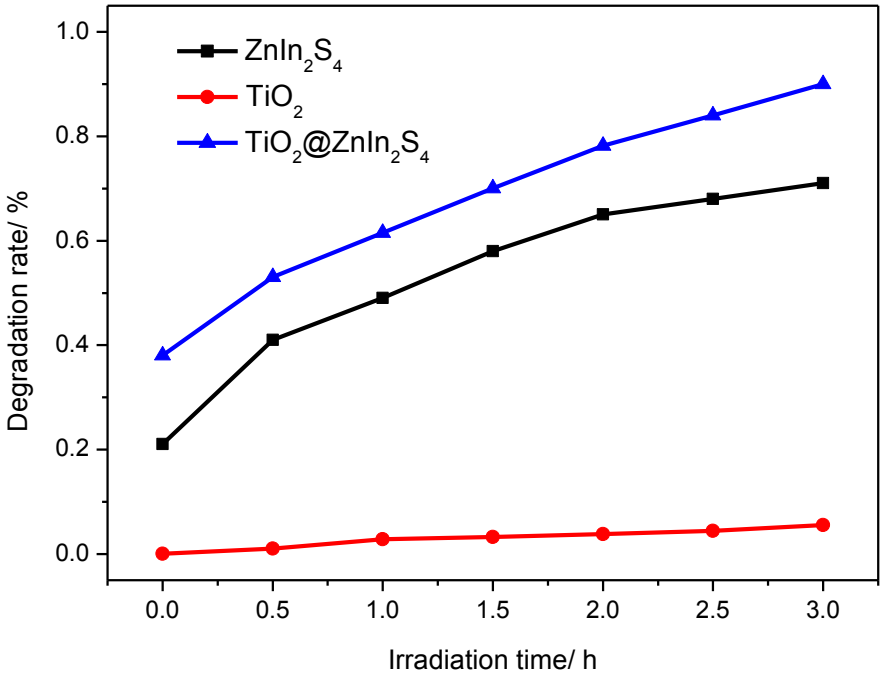

Fig. 7

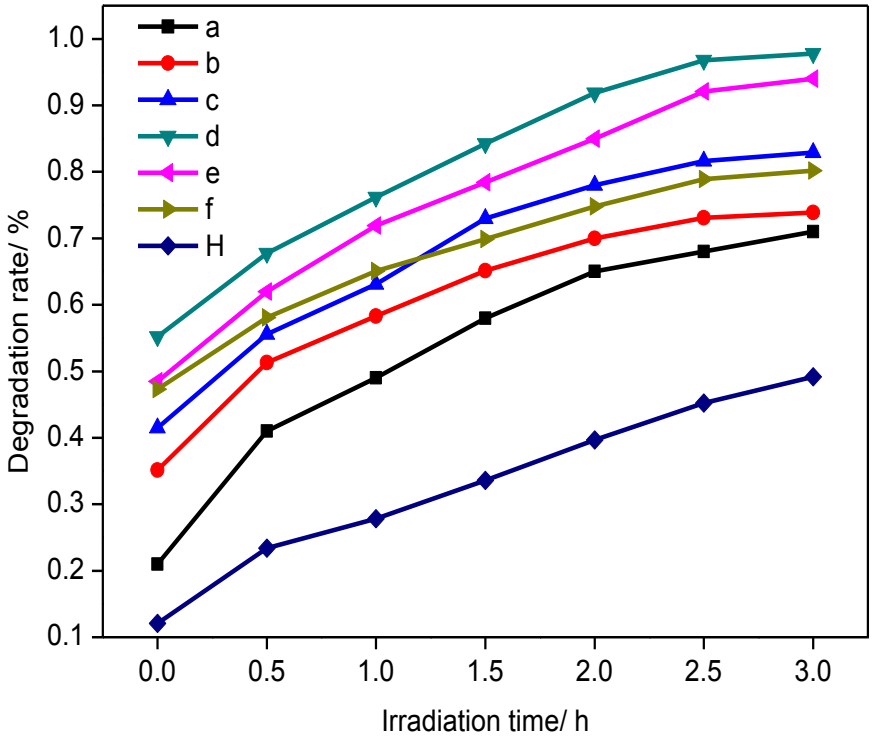

Fig. 8

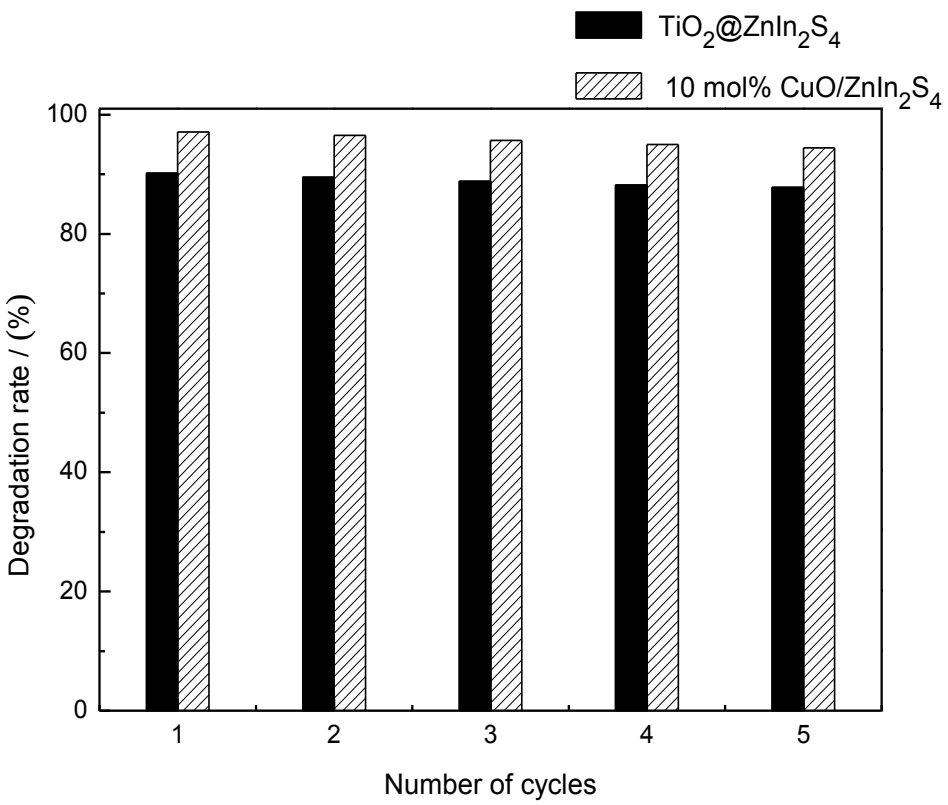

Fig. 9

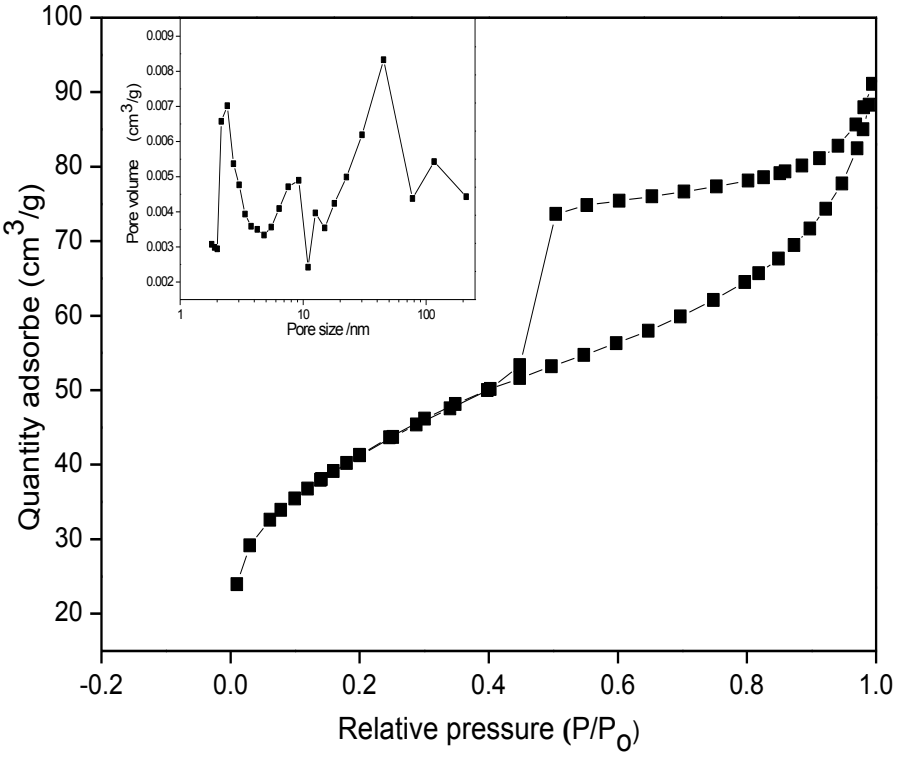

Fig. 10

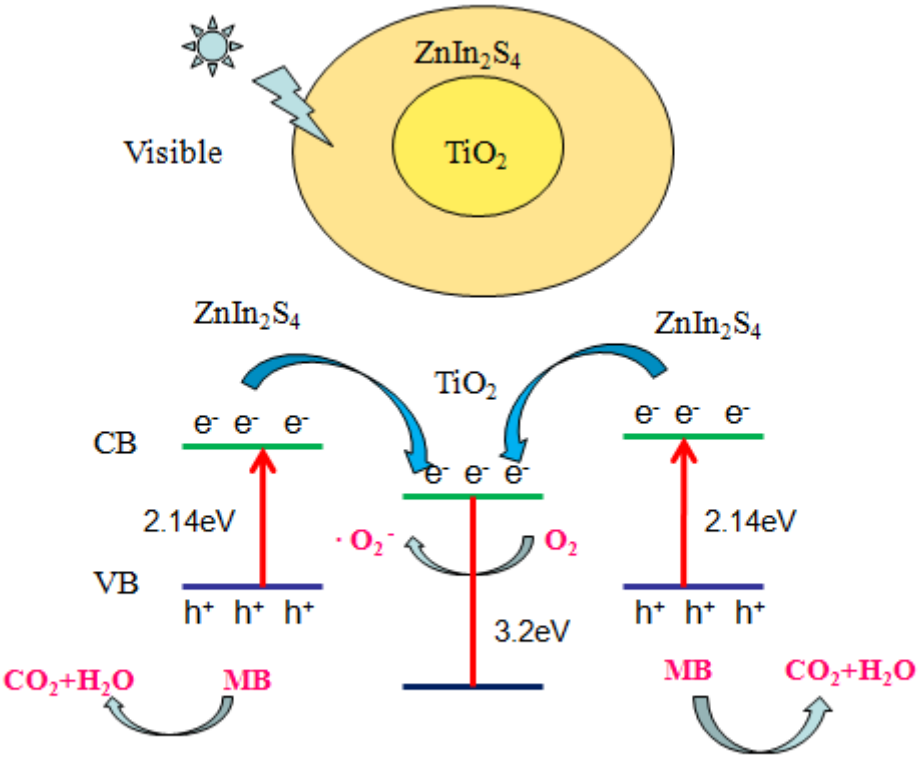

Core-shell coupling

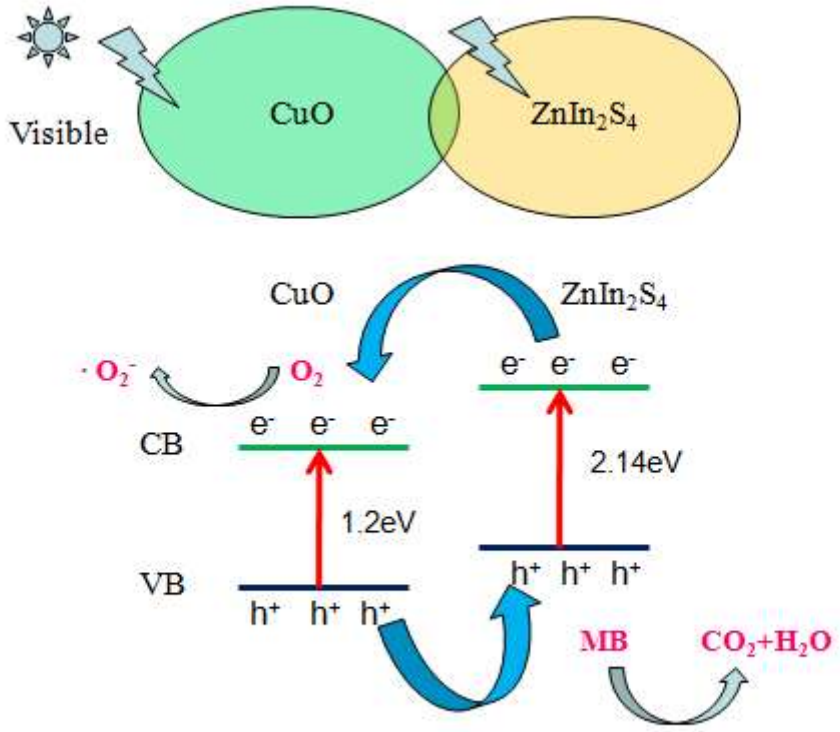

Contact coupling

Table 1 Nitrogen adsorption-desorption isotherm results of variation CuO content series $ZnIn_2S_4$ products

CuO content	0	5%	7%	10%	15%	20%
$S_{BET}/m^2 \cdot g^{-1}$	161.72	143.54	127.35	117.87	108.76	95.83